Journal of Ocean Engineering and Science xxx (xxxx) xxx

Contents lists available at ScienceDirect

Journal of Ocean Engineering and Science

journal homepage: www.elsevier.com/locate/joes

Research Paper

Nonlinear air dynamics of a surface effect ship in small-amplitude waves

Zhiqun Guo[a,b], Liangjing Zhong[a], Kai Wang[a,b,*], Zhiyu Jiang[c]

[a] School of Ocean Engineering and Technology, Sun Yat-Sen University
[b] Southern Marine Science and Engineering Guangdong Laboratory (Zhuhai), Zhuhai 519000, China
[c] Department of Engineering Sciences, University of Agder, Norway

ARTICLE INFO

Article history:
Received 7 October 2022
Revised 27 October 2022
Accepted 24 November 2022
Available online xxx

Keywords:
Surface effect ship
Air dynamics
Nonlinear
Air leakage
Small-amplitude wave
Seakeeping performance

ABSTRACT

In many existing works, the seakeeping motions and air dynamics of a surface effect ship (SES) were assumed to be linear under small-amplitude waves (wave amplitude to wave length ratio $\leq$ 5%) to enhance the computational efficiency. However, according to SES model test results, it was found that even in small-amplitude waves, the fluctuating air cushion pressure shows significantly nonlinear effects. To precisely reveal this distinctive feature, the origin of nonlinearity was carefully investigated and the air leakage was considered as the main source of nonlinearity based on mathematical analysis in this paper. The reason is that the variance of clearance height under seals is comparable to the clearance height at equilibrium state in small-amplitude waves, which makes the air leakage area intermittently equal to zero without any harmonic variance. Therefore, an efficient partial nonlinear numerical model for the SES dynamics was proposed by combining a linear frequency-domain hydrodynamic model based on the efficient 2.5D methods with a nonlinear time-domain air dynamic model. The nonlinear parts of numerical results from the partial nonlinear model, including the fluctuating air pressure and midship accelerations, agree well with experimental results. The results demonstrate the effectiveness of the partial nonlinear model on the SES seakeeping performance prediction, and confirm that its nonlinearity mainly originates from the air leakage.

1. Introduction

The surface effect ship (SES) is a hybrid between hovercraft and catamaran, under which an air cushion is trapped between demihulls and bow/stern seals (skirts). The air cushion allows SES to partially glide on the air layer and thus can substantially reduce the running resistance as well as the wave loads. Generally, due to the interaction between demihull and air pressure hydrodynamics, cushion air dynamics and bow/stern seal dynamics, the seakeeping performance of SES is highly complicated and special phenomenon might arise, such as the cobblestone effect (including acoustic resonance) in short waves [6]. Nonetheless, in middle to long waves with small-amplitudes, the interaction between seals and waves is not significant and dynamic response of seals can also be ignored due to the slowly-varying motion of SES, so one only needs to consider the demihull hydrodynamics, air pressure hydrodynamics and cushion air dynamics [6,8,9,10,21].

The demihull hydrodynamics involves the radiation and diffraction waves/forces due to the interaction between demihulls and waves, which could be evaluated by solving the Neumann boundary condition problems on the wetted surface of demihulls as those on catamarans. Typically, the three-dimensional (3D) linear or nonlinear numerical methods such as URANS method [1,22], finite element method [7] or Rankine source method [2] were exploited to obtain relatively precise hydrodynamics of demihulls. However, the 3D methods are computationally expensive and might be hard to meet the engineering demands such as hydrodynamic optimization. To enhance the computational efficiency, Guo *et al.* [8–10] employed a linear 2.5D method to calculate the hydrodynamic parameters in connection with demihulls of an SES running in small-amplitude waves and obtained satisfactory results. The 2.5D method is highly efficient due to the dimensionality reduction on the control equation and body conditions from 3D to 2D [5,9,10,17], while only the free surface condition remains 3D.

* Corresponding author.
E-mail address: wangkai25@mail.sysu.edu.cn (K. Wang).

https://doi.org/10.1016/j.joes.2022.11.001

The air pressure hydrodynamics refers to the radiation water waves/forces excited by the fluctuating air cushion pressure. In the computational fluid dynamics (CFD) methods, the air pressure hydrodynamics and cushion air dynamics are coupled to each other and need to be simultaneously solved at each time step [1]. Alternatively, in potential theory the air pressure hydrodynamic problem could be deliberately decoupled from the air cushion dynamic problem, and specialized methods can be employed to individually solve the air pressure hydrodynamic problem, e.g., the analytical methods for pressure patches [9,20], 3D Green's function method for zero-speed air cushion supported platform [16], a single-domain 2.5D method [10] or a multi-domain 2.5D method [11] for high-speed SES.

The cushion air dynamics relates to the fluctuating air pressure in the cushion produced by the change in air mass due to air inflow/leakage and in air volume due to the motion of SES and elevation of free surface under the cushion. In cushion air dynamics the control equations and all relevant conditions including air inflow/leakage, SES motion and wave pumping effect, need to be considered. In the potential theory, the control equations for air dynamics commonly could be the nonlinear adiabatic equation [21] with/without the linear Helmholtz equation [6,10,16]. The adiabatic equation connects the air pressure, density, volume and acoustic speed, which is necessary in compressible air flows. The Helmholtz equation is optional, which can differentiate the uneven distribution of air pressure in the cushion and thus is suitable for solving large scale problems [15] or the acoustic resonance problem [6]. The air inflow counts on the characteristics of the fan performance curve, which might be the linear equation [1,6,9,10], or the quadratic one [4,12,21]. The air leakage was modeled using various methods ranging from Bernoulli's equation [6], Euler's equation [12] to Navier-Stokes (NS) equations [13]. According to Hirata and Faltinsen [13], the air leakage model from the incompressible NS equations was compared with the Bernoulli's one, and the viscous effect was found to be not significant under the rigid stern seal bag assumption, which suggests that potential theories are appropriate for modeling the air leakage. Obviously, all the above-mentioned air leakage models are nonlinear due to the possible irregular variance of leakage area and the square root of pressure difference between cushion and atmosphere. Nevertheless, in some works [8-11,14], for the sake of simplicity, the air leakage was linearized based on the assumptions of small wave amplitude and small hull motion amplitude. This simplification might be rational if one only considers the linear seakeeping performance. However, once the wave amplitude is not small enough, or the nonlinear effects of the air dynamics and SES motion become important, the linearized air leakage model will not hold anymore.

According to the experimental results from authors' SES model in small-amplitude waves [8], the heave and pitch responses are almost linearly proportional to wave amplitudes while the fluctuating cushion air pressure, midship accelerations have significant nonlinear effects. It also suggests that the nonlinear effects of the SES should not be neglected and the existing linear models [8–11] are not appropriate for the nonlinear performance prediction. To this end, the source of nonlinearity for the SES will be examined and a novel efficient seakeeping motion prediction model will be developed to take into account the nonnegligible nonlinear effects of the seakeeping performance in this paper. Based on the developed model, the nonlinear air dynamics and motion response of the SES will also be investigated.

The paper is organized as follows. First, the experimental results of the SES model are preprocessed and analyzed in both the time and frequency domain. Then, a partial nonlinear numerical model for the SES seakeeping motion is presented. Finally, the numerical results are compared with the experimental ones to verify the effectiveness of the proposed model, and conclusions are summarized.

2. Results processing of model tests

The SES presented in this paper is also called as partial air cushion supported catamaran (PACSCAT) in Guo *et al.* [8]. The plane projections, 3D model and physical picture of the SES model are illustrated in Fig. 1. The model scale is 1:10. Principal parameters of the SES model are shown in Table 1. The longitudinal position of the center of gravity (COG) is 0.08 m from the midship towards the stern. In the "cushion-on" state, the outside draft at COG reduces to 0.107 m and the inside draft (air cushion side) is only 0.031 m. In the running state, the average trim angle is about 3.45°. The model tests were performed in the towing tank of dimensions 510 m × 6.5 m × 6.8 m, equipped with a flap wave-maker and towing carriage. More details for the SES and model tests, as well as uncertainty analysis can be found in Guo *et al.* [8].

In the model tests, a 16-channal data acquisition device was employed to synchronously record the time series of heave, pitch, fluctuating air pressure in the midship and midship acceleration. Two cases, i.e. the SES runs in two wavelengths ($\lambda = 12,\ 14$m) at speed $U = 5.0$m/s, are chosen in the following study, from which the maximum encountered frequency is 0.777Hz ($\lambda = 12$m). The original experimental data involved high-frequency noise (>20Hz) due to the precision limit of sensors and/or vibrations from other equipments such as fan. A zero-phase lowpass Butterworth filter was exploited to eliminate the high-frequency noise of experimental data without phase distortion, in which the cutoff frequency for the point 3 dB below the passband value was set at 4 Hz (more than 5 times of the maximum encountered frequency). According to our test, the filtered data are not sensitive to the cuttoff frequency varying from 4Hz to larger ones.

Fig. 2(a)-(d) depict the zero-mean experimental data and the processed data on heave (η_3), pitch (η_5), fluctuating air pressure ($\hat{p}$) and midship acceleration ($\ddot{\eta}_{\mathrm{m}}$) obtained from the SES model running under speed $U = 5.0$m/s in waves of length $\lambda = 12$m, respectively. Though for each speed and wavelength, the test lasted for about 30 s, only 6 seconds' steady-state test data were used for analysis. To avoid confusion, the starting time of the data was set to 0 rather than the original one. In the figures, the green dot dash lines labeled by "Original" are the original experimental results. The black lines labeled by "Filtered" are the processed experimental results filtered using the zero-phase low-pass Butterworth filter, and the red dash lines labeled by "Sinusoidal" are the results by sinusoidal curve fitting. From Fig. 2(b), (d) one notes that the original data are quite noisy and it is hard to observe the real shape before preprocessing, while the heave and fluctuating air pressure data (Fig. 2(a), (c)) have relatively less noise. One can also notice that the "Sinusoidal" and "Filtered" curves almost coincide with each other in Fig. 2(a)-(b), which suggests that the heave and pitch motion are perfectly linear. In contrast, as shown in Fig. 2(c)-(d), the "Filtered" curves that are significantly different from the "Sinusoidal" ones, revealing the nonlinear effects on the fluctuating air pressure and midship acceleration.

To reduce the truncation effect on the Fourier transform of time domain series with limited length, the filtered experimental data were preprocessed by the Hann window [18]. Fig. 3(a)-(d) further depict the discrete Fourier transform of the preprocessed experimental data. In Fig. 3(a) and (b) one can only find a main peak for heave and pitch response at the encountered frequency f_0, respectively, while high frequency peaks are not significant. On the other hand, in Fig. 3(c) and (d) one can clearly observe at least 2 peaks for the fluctuating air pressure and midship acceleration occuring at the base frequency (encountered frequency) f_0, double frequency $2f_0$, respectively, and higher frequencies are even visible.

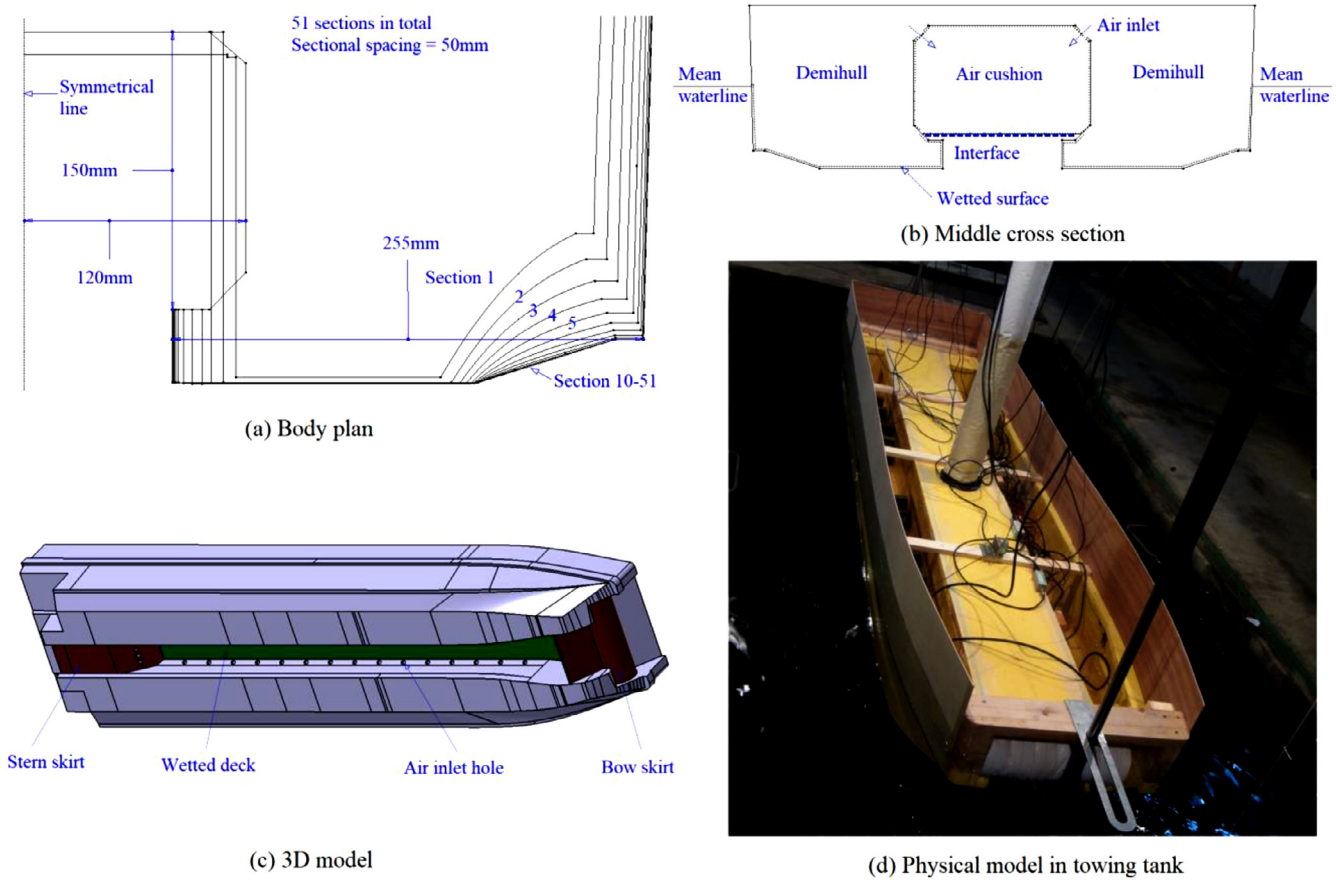

Fig. 1. The plane projections, 3D model and physical picture of the SES model.

Table 1
Principal parameters of the SES model [8].

Parameters	Value	Parameters	Value
Model scale	1:10	Moment of inertia for pitch (I_{yy})	77.4 kg·m^2
Mass (M)	145 kg	Model running speed (U)	5.0m/s
Overall length (L)	3.0 m	Static cushion overpressure (p_0)	510 Pa
Beam (B)	0.7 m	Air inflow rate (Q_0)	150 m^3/h
Cushion length (l)	2.5 m	Wave amplitude (η_0)	0.025 m
Cushion breadth (b)	0.24 m	Air density (25 °C) (ρ_a)	1.185 kg/m^3
Water density (ρ_w)	1000 kg/m^3	Proportion of air cushion displacement	21.5%

Comparing Fig. 3(c) and (d), one notes that the relative magnitude of the fluctuating air pressure at $2f_0$ is larger than that of the midship acceleration, i.e. $\hat{p}(2f_0)/\hat{p}(f_0) > \ddot{\eta}_m\ (2f_0)/\ddot{\eta}_m\ (f_0)$, which indicates that the nonlinear effects on midship acceleration are not as strong as the fluctuating air pressure.

The distinctive nonlinear features of the air pressure and the motion response should result from the small displacement proportion of the air cushion (only 33% of the SES displacement), which reduces the influence of the fluctuating air pressure on the SES motions. Thereby, in our previous works [8–11], only the linear models were applied to predict the seakeeping motions. Once the displacement of the air cushion contributes to a larger proportion, e.g., 80%, the motions of the SES show significant nonlinear effects, which requires more appropriate models for analysis. To address the issue, a partial nonlinear model consiting of nonlinear air dynamic model and linear hydrodynamic model will be developed to ensure that the main futures of the nonlinear effect can be taken into account without increasing significantly the computational burden.

3. Partial nonlinear equations for the SES seakeeping motion

To analyze the nonlinear features of the air dynamics and SES seakeeping performance, a partial nonlinear model is established in this section by combining a frequency-domain linear hydrodynamic model and a time-domain nonlinear air dynamic model.

As shown in Fig. 4, $O-XYZ$ is an earth-fixed coordinate system, and $o-xyz$ is an SES-accompanied coordinate system always parallel to $O-XYZ$. When the SES is located at its mean position, the x-axis is pointing towards the bow parallel to the longitudinal plane of the SES and the z-axis is pointing vertically upward through the COG of the SES. The origins of both coordinate systems are in the plane of the mean free surface.

3.1. Nonlinear air dynamics of the SES

As shown in Fig. 5, the air dynamics is affected by air inflow, air leakage, SES motion and elevation of free surface under the cushion. According to the discussion, the air inflow, SES motion and

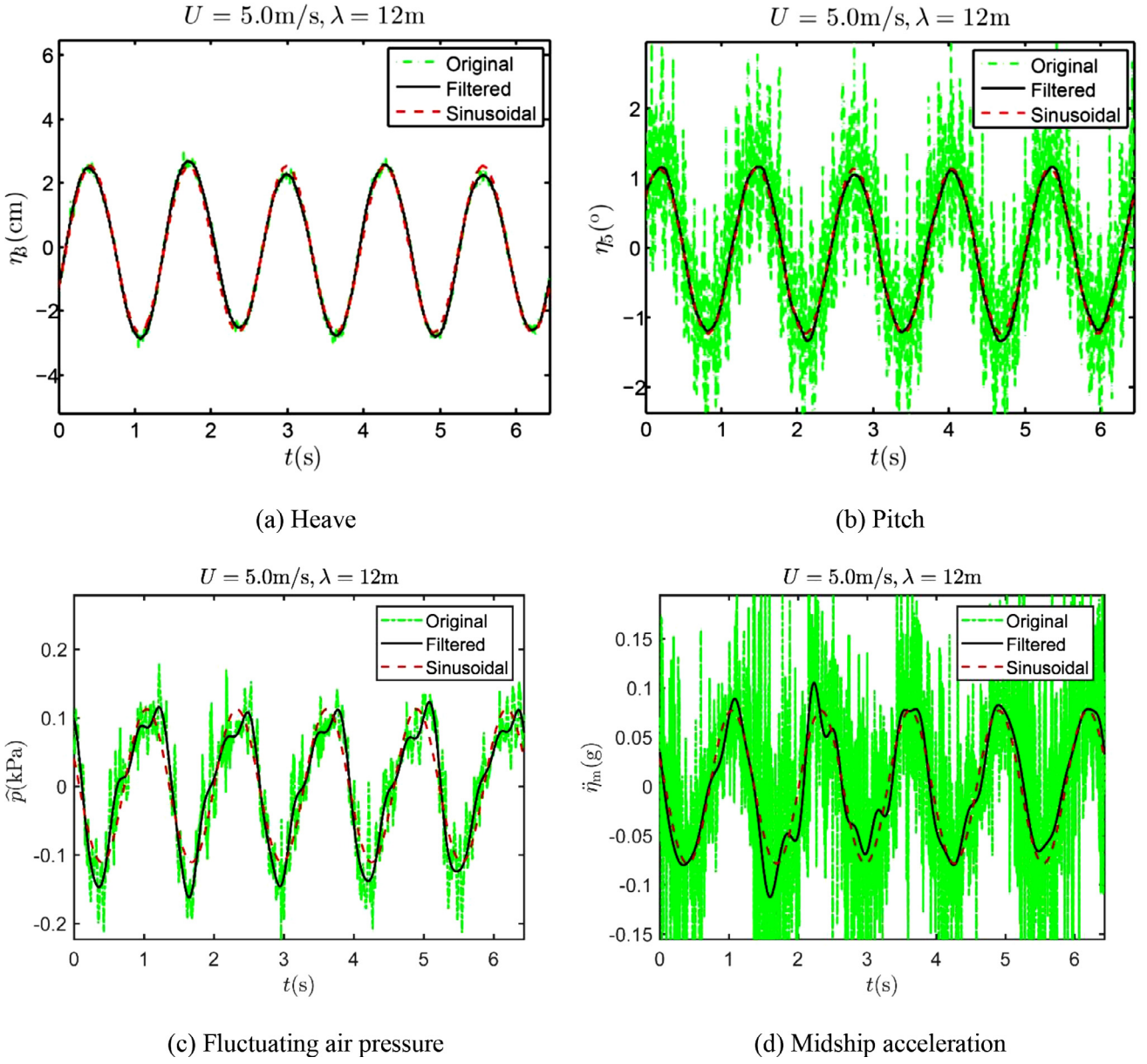

Fig. 2. Time series of experimental results and the processed data on seakeeping performance of the SES running with speed $U = 5.0\text{m/s}$ and in waves of length $\lambda = 12\text{m}$. 'Original' refers to the original data recorded in model tests. 'Filtered' refers to the data obtained by filtering the original data using a zero-phase lowpass Butterworth filter, whose cutoff frequency was set at 4 Hz. 'Sinusoidal' refers to the sinusoidal curve fitted results for the filtered curve. The unit for midship acceleration is the gravitational acceleration (g).

elevation of free surface under the cushion are initially assumed to be linear, while the air leakage is nonlinear. For simplicity, the framework of air dynamic model and its linear components similar to Guo *et al.* [8] are given in **Appendix A**, and here we only present the nonlinear air leakage model that is different from the one in Guo et al. [9–11].

Based on the Newton's second law of motion and using the infinitesimal method, one gets Euler's equation for the ideal fluid [12]

$$\frac{\mathrm{d}p}{\rho} + v\mathrm{d}v + \mathrm{g}\mathrm{d}z = 0 \tag{1}$$

where p, ρ, v, z are the pressure, density, velocity, height of a particle of the ideal fluid, respectively.

Combining Eq. (A1) and Eq. (1) and ignoring the gravity of air and its flow speed in the cushion, the Bernoulli equation for adiabatic compressible flow can be written as

$$\left(\frac{\gamma}{\gamma-1}\right)\frac{\hat{p}(x,y,t)+p_0+p_\mathrm{a}}{\hat{\rho}_\mathrm{a}} = \left(\frac{\gamma}{\gamma-1}\right)\frac{p_\mathrm{a}}{\rho_\mathrm{a}} + \frac{v_a^2}{2} \tag{2}$$

where $\hat{p}(x,y,t)$, p_0, p_a are the section-averaged fluctuating air cushion pressure, mean overpressure of air cushion and atmosphere pressure, respectively; $\hat{\rho}_\mathrm{a}$, ρ_a the air density in the cushion and atmosphere, respectively; $\gamma = 1.4$ is the ratio of specific heat capacities for air; v_a the air flow velocity.

Using the pressure-density relationship Eq. (A1), with the consideration of Eq. (A3), $\hat{\rho}_\mathrm{a}$ can be eliminated and Eq. (2) becomes

$$\frac{v_a^2}{2} \cong \frac{p_0}{\rho_\mathrm{a}} \tag{3}$$

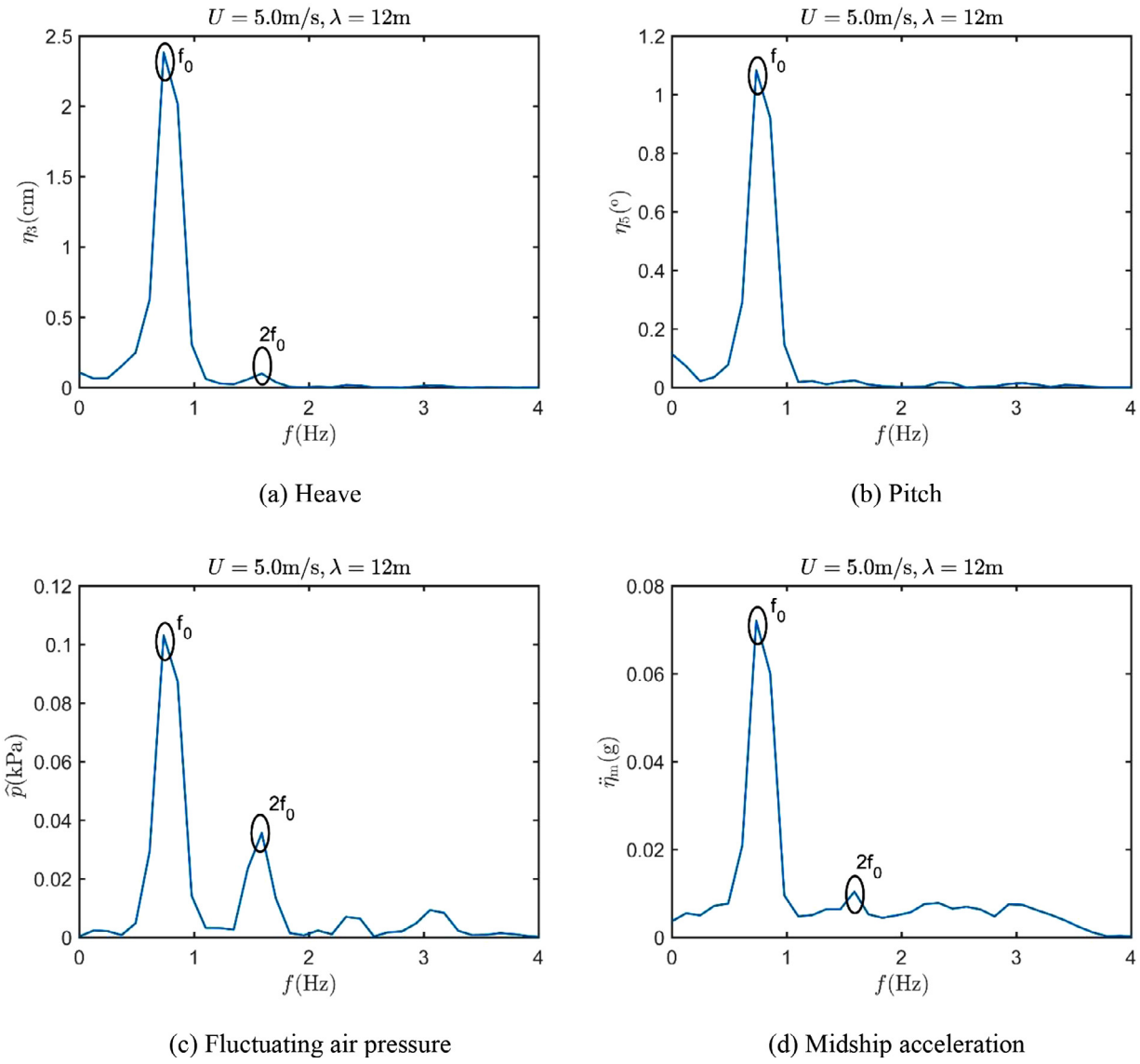

Fig. 3. The Fourier transform on the preprocessed experimental results from the SES running with speed $U = 5.0\text{m/s}$ and in waves of length $\lambda = 12\text{m}$. f_0 is the encountered frequency for the SES. The responses more than 4Hz are truncated.

From Eq. (3) one gets the expression for air leakage from the cushion

$$Q^{\text{out}}(t) = \left(C_f H\left[h_f(t)\right] + C_a H[h_a(t)]\right) b\sqrt{2p_0/\rho_a} \tag{4}$$

where:

(1) $H[x]$ considers the shutdown effect for air leakage, which is the real clearance height for leakage defined as

$$H[x] = \begin{cases} x, & x > 0 \\ 0, & x \le 0 \end{cases} \tag{5}$$

Obviously, $H[x]$ is an unsmoothed function and is the only factor that makes the air leakage (Eq. (4)) nonlinear. We did try to smooth the function $H[x]$ but found no significantly different results can be obtained as compared to Eq. (5).

(2) $C_f, C_a$are the flow contraction coefficient for bow and stern seal leakage, respectively, which are recommended to be set as $C_f = 0.6,\ C_a = 1.0$ [1,6].

(3) $h_f(t),\ h_a(t)$ are the section-averaged clearance from the interface between air cushion and water (hereinafter referred to as interface) to the underneath of bow and stern seal, respectively:

$$h_f(t) = h_{f0} + \hat{h}_f(t) = h_{f0} + \eta_3(t) + (y_m - y_g)\eta_4(t) - \left(x_f - x_g\right)\eta_5(t) - \bar{\zeta}\left(x_f, t\right) \tag{6}$$

$$h_a(t) = h_{a0} + \hat{h}_a(t) = h_{a0} + \eta_3(t) + (y_m - y_g)\eta_4(t) - (x_a - x_g)\eta_5(t) - \bar{\zeta}\left(x_a, t\right) \tag{7}$$

where

(3.1) $\bar{\zeta}(x,t)$ is the section-averaged interface elevation defined as

$$\bar{\zeta}(x,t) = \frac{1}{b}\int_{y_m - b/2}^{y_m + b/2} \zeta(x,y,t)\mathrm{d}y \tag{8}$$

where y_m is the transversal center of the air cushion.

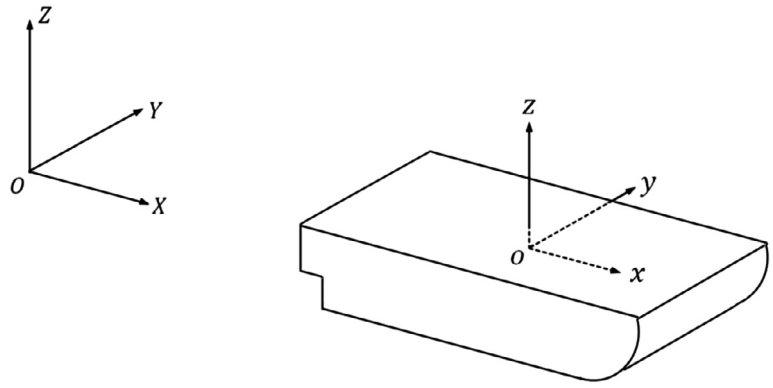

Fig. 4. Sketch of the coordinate systems.

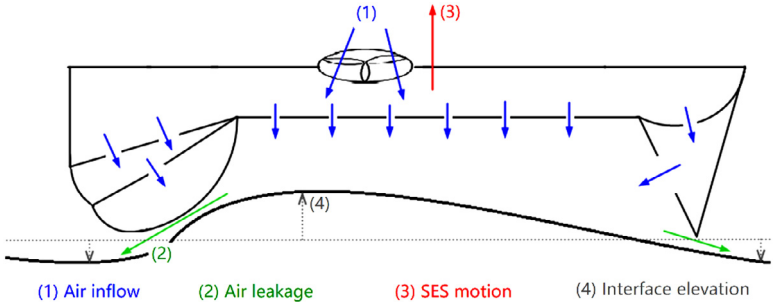

Fig. 5. The air dynamics of the SES is affected by ① air inflow, ② air leakage, ③ motions of the SES and ④ elevation of interface under the air cushion.

(3.2) x_f, x_a are the x-coordinate of the bow and stern seal, respectively;

(3.3) h_{f0}, h_{a0} are the steady clearance height for the bow and stern seal leakage, respectively, which satisfy the following condition

$$Q_0 = \left(C_f h_{f0} + C_a h_{a0}\right) b\sqrt{2p_0/\rho_a} \tag{9}$$

(3.4) $\eta_3(t), \eta_4(t), \eta_5(t)$ are the heave, roll and pitch of the SES, respectively.

Using the parameters from Table 1, one can estimate the steady clearance height for the test model to be $|h_{f0}|, |h_{a0}| \leq$ 1cm. On the other hand, according to the model tests one found $|\hat{h}_f(t)|$ and $|\hat{h}_a(t)|$ can reach the level of 2.5cm, and $h_f(t)$ and $h_a(t)$ may change their signs as the motions of the ship model and waves. So the air leakage equation (Eq. (4)) is nonlinear due to $H[h_f(t)]$, $H[h_a(t)]$. This is the main different from Guo *et al.* [10], which uses a linearized air leakage model. Another difference from Guo *et al.* [10] is that the equations of the air dynamics are in established the time domain here, while those in Guo *et al.* [10] were established in the frequency domain.

3.2. Hydrodynamics of the SES

For completeness, the linear potential methods for solving the wave and ship motion dynamics are described in this subsection. More detailed are referred to Guo *et al.* [10]. Since the depth of towing tank is 7 m, which is not less than the half wavelength of incident waves, the incident waves can be deemed as deep water waves with potential

$$\phi_I = \eta_0 Re\left\{\tilde{\phi}_0(x,y,z,t)\right\} = \eta_0 Re\left\{\frac{\mathrm{i}g}{\omega_0} e^{k_0 z} e^{\mathrm{i}(\omega t - k_0(x\cos\theta + y\sin\theta))}\right\} \tag{10}$$

with

$$\omega = \omega_0 - k_0 U\cos\theta \tag{11}$$

where $Re\{z\}$ takes the real part of complex z; i is the imaginary number, η_0 the wave amplitude, $\tilde{\phi}_0(x,y,z,t)$ the incident potential with unit amplitude, ω the encountered frequency, ω_0 the natural frequency, k_0 the wave number, θ the incident wave angle.

Within the framework of linear assumption, the unsteady disturbance potentials can be written as

$$\begin{cases} \phi_R = \sum_{j=1}^{6} \eta_j(t)\phi_j(x,y,z) = \sum_{j=1}^{6} Re\left\{\tilde{\eta}_j\tilde{\phi}_j(x,y,z)e^{\mathrm{i}\omega t}\right\} \\ \phi_D = \eta_0\phi_7(x,y,z,t) = \eta_0 Re\left\{\tilde{\phi}_7(x,y,z)e^{\mathrm{i}\omega t}\right\} \\ \phi_P = \eta_8(t)\phi_8(x,y,z) = Re\left\{\tilde{\eta}_8\tilde{\phi}_8(x,y,z)e^{\mathrm{i}\omega t}\right\} \end{cases} \tag{12}$$

where $\phi_j(x,y,z,t)(j=1,\ldots,6)$ is the radiation potential due to unit-amplitude motion of j-th degree; $\phi_7(x,y,z,t)$ the diffraction potential due to incident wave of unit amplitude; $\phi_8(x,y,z,t)$ the radiation potential due to the unit-amplitude fluctuating air pressure in the first mode; $\tilde{\eta}_j(j=1,\ldots,6)$ the complex amplitude of j-th degree of motion; $\tilde{\eta}_8$ the complex amplitude of the fluctuating air pressure in the first mode; $\tilde{\phi}_j(x,y,z)(j=1,\ldots,6)$ the spatial component of the radiation potential due to unit amplitude motion of j-th degree; $\tilde{\phi}_8(x,y,z)$ the spatial component of the radiation potential due to the unit amplitude fluctuating air pressure in the first mode.

The potential $\tilde{\phi}_j(x,y,z)(j=2,\ldots,7)$ can be calculated by solving the Neumann boundary value problem using the classical 2.5D method [8,17], while the potential $\tilde{\phi}_8(x,y,z)$ by solving the mixed boundary value problem using the 2.5D method that was firstly developed by Guo *et al.* [10]. The potential $\tilde{\phi}_1(x,y,z)$ is approximated to zero according to the slender body assumption of the 2.5D method. Details for obtaining $\tilde{\phi}_j(x,y,z)(j=2,\ldots,8)$ are not given in this paper.

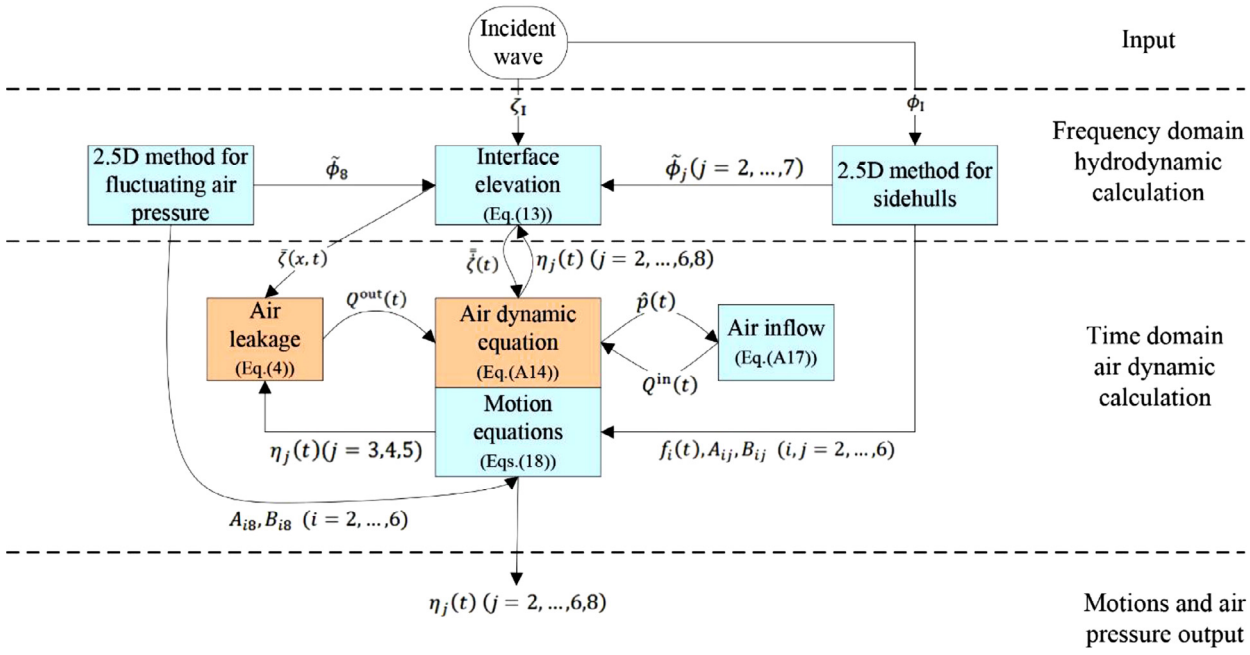

Fig. 6. Numerical flowchart for solving the motions and fluctuating air cushion pressure, where the air leakage model and air dynamic equation (in brown color) are nonlinear, while the rest models or equations (in blue color) are linear.

Once the complex potentials $\tilde{\phi}_j(x,y,z)(j=2,\ldots,8)$ are solved, the interface elevation in Eq. (A15) can be evaluated by

$$\zeta(x,y,t)=\eta_8(t)+\zeta_I(x,y,t)+\zeta_R(x,y,t)+\zeta_D(x,y,t)+\zeta_P(x,y,t) \tag{13}$$

with

$$\zeta_I(x,y,t)=-\frac{\eta_0}{g}Re\left\{\left(\frac{\partial}{\partial t}-U\frac{\partial}{\partial x}\right)\phi_0(x,y,0,t)\right\} \tag{14}$$

$$\begin{aligned}\zeta_R(x,y,t)&=-\frac{1}{g}Re\left\{\sum_{j=2}^{6}\tilde{\eta}_j e^{i\omega t}\left(i\omega-U\frac{\partial}{\partial x}\right)\tilde{\phi}_j(x,y,0)\right\}\\&\cong-\frac{1}{g}\sum_{j=2}^{6}\left(\eta_j(t)Re\left\{\left(i\omega-U\frac{\partial}{\partial x}\right)\tilde{\phi}_j(x,y,0)\right\}\right.\\&\quad\left.+\frac{1}{\omega}\dot{\eta}_j(t)\mathrm{Im}\left\{\left(i\omega-U\frac{\partial}{\partial x}\right)\tilde{\phi}_j(x,y,0)\right\}\right)\end{aligned} \tag{15}$$

$$\begin{aligned}\zeta_D(x,y,t)&=-\frac{\eta_0}{g}Re\left\{e^{i\omega t}\left(i\omega-U\frac{\partial}{\partial x}\right)\tilde{\phi}_7(x,y,0)\right\}\\&=-\frac{\eta_0}{g}\left(\cos(\omega t)Re\left\{\left(i\omega-U\frac{\partial}{\partial x}\right)\tilde{\phi}_7(x,y,0)\right\}\right.\\&\quad\left.-\sin(\omega t)\mathrm{Im}\left\{\left(i\omega-U\frac{\partial}{\partial x}\right)\tilde{\phi}_7(x,y,0)\right\}\right)\end{aligned} \tag{16}$$

$$\begin{aligned}\zeta_P(x,y,t)&\cong-\frac{1}{g}\left(\eta_8(t)Re\left\{\left(i\omega-U\frac{\partial}{\partial x}\right)\tilde{\phi}_8(x,y,0)\right\}\right.\\&\quad\left.+\frac{1}{\omega}\dot{\eta}_8(t)\mathrm{Im}\left\{\left(i\omega-U\frac{\partial}{\partial x}\right)\tilde{\phi}_8(x,y,0)\right\}\right)\end{aligned} \tag{17}$$

In Eqs. (15) and (17), the approximate equals signs mean that unsteady waves might not be harmonic if $\eta_j(t)$ is not sinusoidal, though the potentials are solved in the frequency domain. In contrast, within the linear framework the unsteady waves are always harmonic, as suggested in Guo *et al.* [10].

3.3. Equations of motion of the SES

As mentioned above, the 2.5D method for hydrodynamics of the SES cannot consider the surge motion, so the time-domain equations of motion of the SES are 5-DOF that can be formulated as

$$\sum_{j=2}^{8(j\neq7)}\left(\left(M_{ij}+A_{ij}\right)\ddot{\eta}_j(t)+B_{ij}\dot{\eta}_j(t)+C_{ij}\eta_j(t)\right)=f_i(t),\ \ i=2,\ldots,6 \tag{18}$$

where M_{ij}, A_{ij}, B_{ij}, C_{ij} are the inertia of the SES, added mass, damping, restoring force matrix, respectively, and $M_{ij}=0$ for $j>6$; $f_i(t)$ the wave force along the i-th direction.

The coefficients A_{ij}, B_{ij}, C_{ij} are stationary, where A_{ij}, B_{ij} are obtained through the following equations ($i=2,\ldots,6$; $j=2,\ldots,6,8$)

$$\begin{cases}A_{ij}=Re\{\Lambda_{ij}\}/\omega^2\\B_{ij}=-\mathrm{Im}\{\Lambda_{ij}\}/\omega\end{cases} \tag{19}$$

$$\Lambda_{ij}=-i\omega\rho_w\iint_{S_B}\tilde{\phi}_j n_i ds+\rho_w U\iint_{S_B}\tilde{\phi}_j m_i ds-\rho_w U\int_{C_A}\tilde{\phi}_j n_i dl \tag{20}$$

where $\mathrm{Im}\{z\}$ takes the imaginary part of complex z, C_A is the stern section of the SES, S_B the wetted surface of SES demihulls, $n_i(i=2,\ldots,6)$ the generalized normal vector, and m_j is defined as $(m_1,m_2,m_3)=(0,0,0)$ and $(m_4,m_5,m_6)=(0,n_3,-n_2)$. It is worthy mentioning that in traditional potential theories, the added mass and damping coefficients of the time-domain motion equations are obtained by calculating the impulse response function (IRF) for the vessel and then applying that IRF at each time step using a convolution integral to account for the past motion of the vessel [3]. The added mass and damping coefficients obtained using the IRF obviously consider both of the transient and steady effect of vessel motions. However, according to the model test data selected for study (see Fig. 2), the waves and motions of the SES are already under steady state. So only the steady part of the

added mass and damping coefficients is considered in this work, which allows one to directly employ the added mass and damping coefficients obtained using the 2.5D method for the time-domain motion equations.

C_{i8} appears due to the fluctuating air pressure acting on the wetted deck:

$$C_{i8} = \rho_{\mathrm{w}} g \iint_{S_{\mathrm{D}}} n_i(x, y)\mathrm{d}x\mathrm{d}y \tag{21}$$

The wave force $f_i(t)$ could be decomposed into

$$f_i(t) = \cos(\omega t)Re\{F_i\} - \sin(\omega t)\mathrm{Im}\{F_i\} \tag{22}$$

$$F_i = F_i^{\mathrm{I}} + F_i^{\mathrm{D}} \tag{23}$$

where F_i^{I}, F_i^{D} are the Froude–Krylov force, diffraction force, respectively. Their expressions are given as follows

$$\begin{cases} F_i^{\mathrm{I}} = -\eta_0 \cdot \mathrm{i}\rho_{\mathrm{w}}\omega_0 \iint_{S_{\mathrm{B}}} \tilde{\phi}_0 n_i \mathrm{d}s \\ F_i^{\mathrm{D}} = \eta_0 \cdot \Lambda_{i7} \end{cases} \tag{24}$$

Nonlinear Eq. (A14) and linear Eqs. (18) are the partial nonlinear motion equations for the SES, from which all degrees of motions (except surge motion) and the fluctuating air pressure $\eta_j(t)(j = 2, \ldots, 6, 8)$ were solved using the 4th order Runge-Kutta method with adaptive time steps.

From the deduction, one finds why air leakage is the main resource of nonlinear effects for the SES. Under the small-amplitude wave condition, the hydrodynamics of the SES demihulls can be solved using the linear 2.5D method [8]. The fluctuating air pressure in the cushion can be modeled using the linear Helmholtz equation with consideration of boundary conditions including air inlet, SES motion, air leakage and interface elevation. The air inflow rate approximately linearly varies with the fluctuating air pressure.

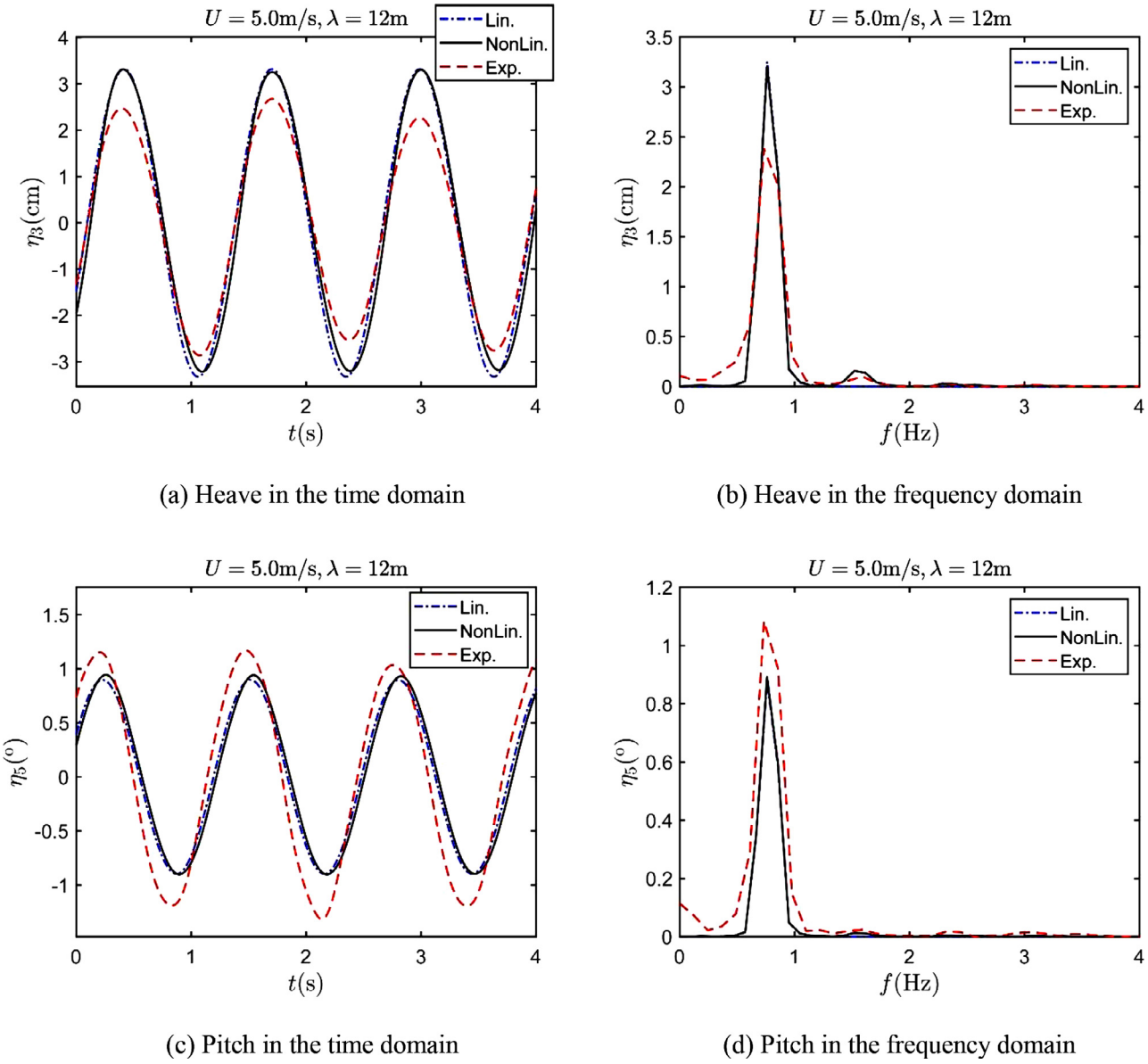

(a) Heave in the time domain

(b) Heave in the frequency domain

(c) Pitch in the time domain

(d) Pitch in the frequency domain

Fig. 7. Comparison of nonlinear numerical results (labeled by 'NonLin.') obtained from the partial nonlinear model to the linear numerical ones (labeled by 'Lin.') and experimental ones (labeled by 'Exp.') with the SES model running speed $U = 5.0$m/s in head waves of wavelength $\lambda = 12$m. Both of numerical results and experimental data were filtered using a zero-phase lowpass Butterworth filter to eliminate the high frequency ($f \geq 4$Hz) noise.

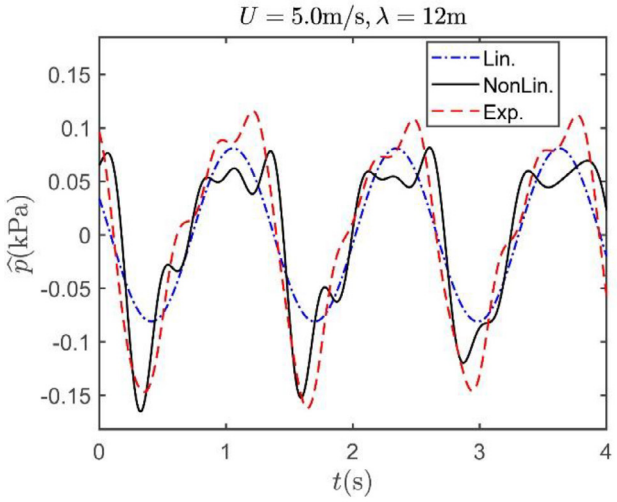

(e) Fluctuating air pressure in the time domain

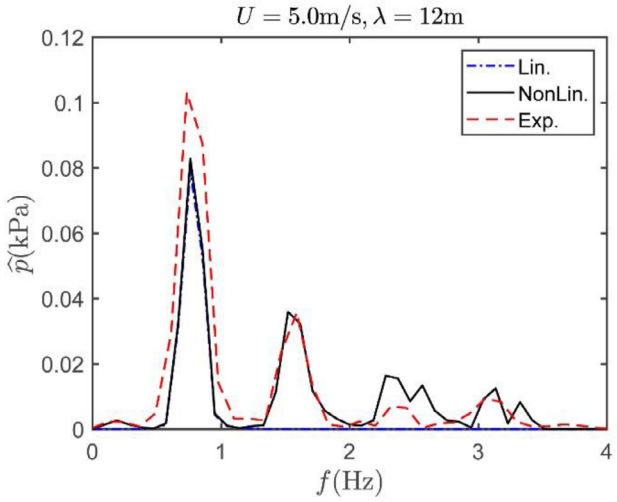

(f) Fluctuating air pressure in the frequency domain

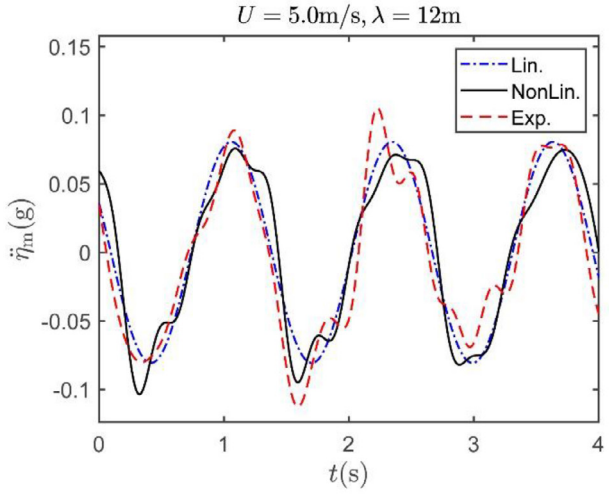

(g) Midship acceleration in the time domain

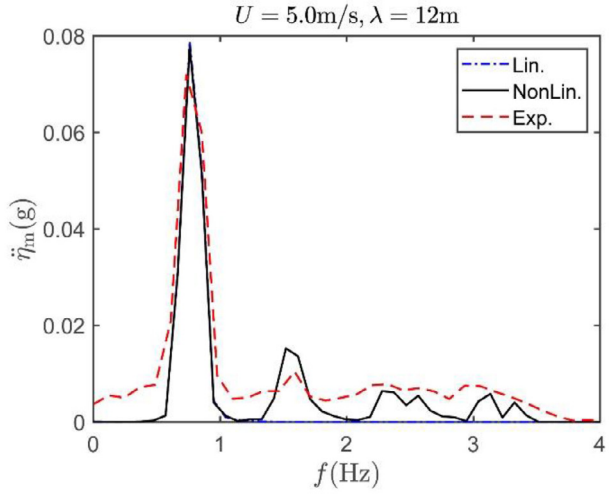

(h) Midship acceleration in the frequency domain

Fig. 7. Continued

The interface elevation could be solved using linear 2.5D method (Guo *et al.*, 2018). The SES motion should be solved by the combination of demihull hydrodynamics and air dynamics, which is not the origin of nonlinearity. However, the height of air leakage clearance at steady state is comparable to even less than the wave amplitude or heave amplitude of the SES, which makes shutdown effect for air leakage clearance in waves. Thus, the air leakage is inevitable nonlinear and makes the whole SES dynamics nonlinear.

Fig. 6 depicts the numerical flowchart for solving the motions and fluctuating aircushion pressure (Eq. (A14) and Eqs. (18)) in the time domain, in which the hydrodynamic coefficients were directly obtained using the 2.5D method in the frequency domain due to that the incident waves are monochromatic and only the steady effect of the SES motions is considered here. From the figure one can observe that the hydrodynamic parameters A_{ij}, B_{ij} $(i = 2, 3, \ldots, 6; j = 2, 3, \ldots, 6, 8)$ in Eqs. (18) were solved in frequency domain as in Guo *et al.* [10], which do not vary with time. The time domain wave force $f_i(t)$ was obtained from Eq. (22) by solving the wave force F_i in the frequency domain and taking the real part of $F_i e^{i\omega t}$. The averaged interface elevation velocity $\overline{\dot{\zeta}}(t)$ in Eq. (A14) was based on potentials $\dot{\phi}_j(x, y, z)(j = 2, \ldots, 8)$, which were also solved in frequency domain. After solving all hydrodynamic coefficients (A_{ij}, B_{ij}, $f_i(t)$), the motions and the fluctuating air pressure $\eta_j(t)(j = 2, \ldots, 6, 8)$, which require relatively less computational efforts, are solved in the time domain. To differentiate, the nonlinear air leakage and air dynamic equation blocks in the flowchart are in brown color, while the linear model blocks are in blue color.

4. Numerical results and discussion

In this section, numerical results obtained from the partial nonlinear model are investigated and compared with experimental data selected from the SES model running in two wavelengths ($\lambda = 12,\ 14\text{m}$) at speed $U = 5.0\text{m/s}$. The wave probe in model tests was fixed near the wavemaker and did not move with the SES model, which makes the phase of SES motions with respect to waves unknown. Thereby, the phase of heave motion rather than wave is set as the benchmark in the following analysis. Similar to

filtering the experimental data, the numerical results were also filtered using a zero-phase lowpass Butterworth filter to eliminate the noisy component of frequency larger than 4 Hz.

4.1. The comparison of numerical and experimental results

The numerical results (black lines labeled by 'NonLin.') obtained from the partial nonlinear model are compared with the linear ones obtained from the linear model (blue dot dash lines labeled by 'Lin.') and the experimental ones (red dash lines labeled by 'Exp.') under the condition that the SES model runs with speed $U = 5.0\text{m/s}$ in head waves of wavelength $\lambda = 12\text{m}, 14\text{m}$, as shown in Fig. 7, Fig. 8, respectively. The linear model is obtained by turning off the shutdown effect of air leakage in the partial nonlinear model, i.e. setting $H[x] = x$ in Eq. (5). To clearly demonstrate the linear and nonlinear components of the time-domain results, the time series was preprocessed firstly by the Hann window [18] to reduce the truncation effect, and then were processed using discrete Fourier transform to obtain the frequency-domain results.

From Fig. 7(a)∼(d) one notes that the heave and pitch response from nonlinear numerical results are very close to the linear ones, and only a very small amplitude of double-frequency nonlinear heave response appears, which desirably corresponds with the experimental one. In Fig. 7(e), (f) the nonlinear numerical results on the fluctuating air pressure agree well with the experimental ones, where the fluctuating air pressure reveals significant nonlinear effects, including not only the double-frequency response, but also the triple and quadruple-frequency ones. Obviously, the linear numerical results can not capture these nonlinear properties at all. Moreover, one notices that in Fig. 7(e) the time series of the fluctuating air pressure have sharp troughs and flat crests with several hollows, which should result from the shutdown effect of air leakage given by Eqs. (4)-(5). Comparing Fig. 7(e) with Fig. 7(a) it can be found the sharp troughs of the fluctuating air pressure occur at the crests of heave, which suggests that the air pressure quickly

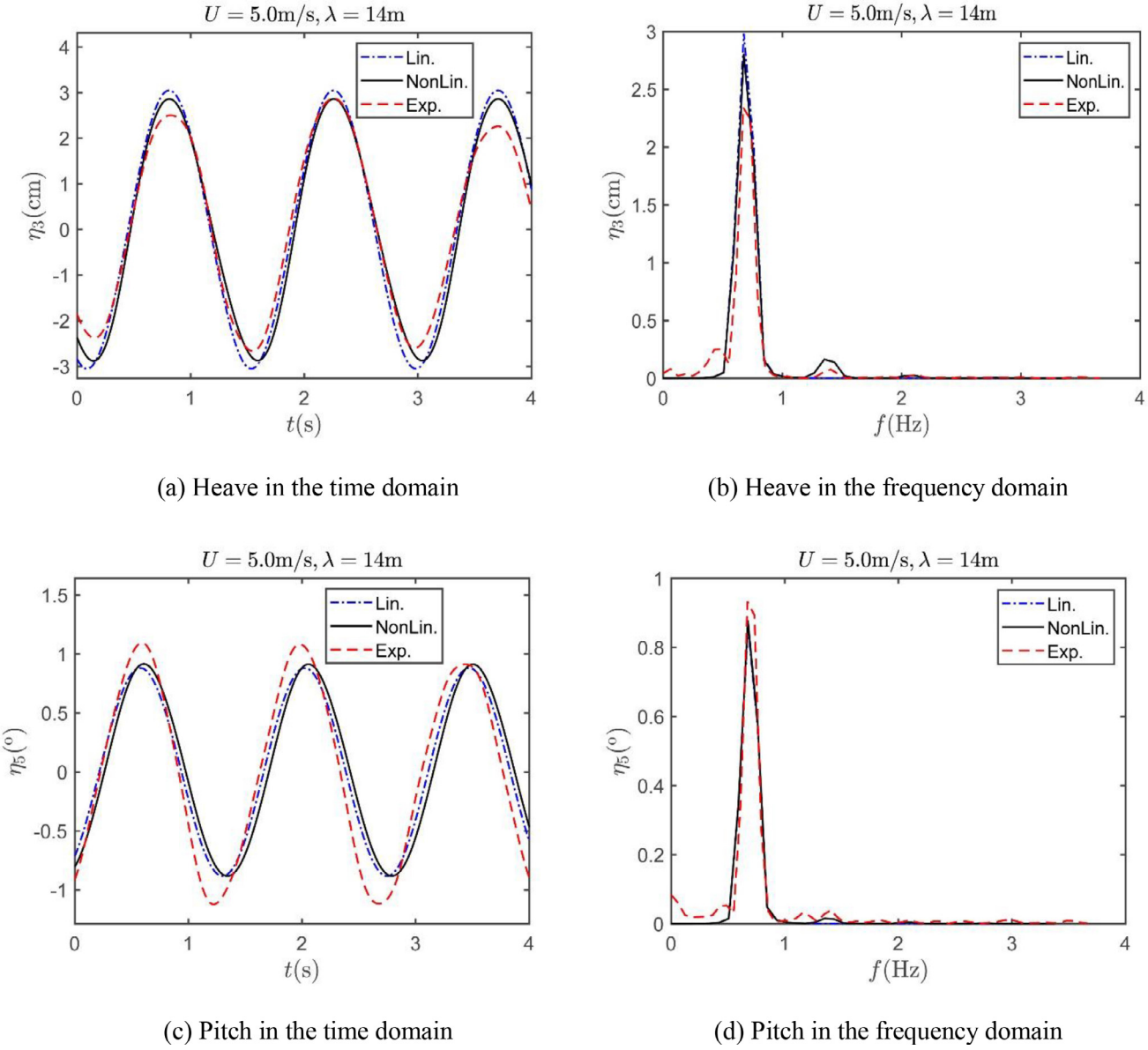

(a) Heave in the time domain

(b) Heave in the frequency domain

(c) Pitch in the time domain

(d) Pitch in the frequency domain

Fig. 8. Comparison of nonlinear numerical results (labeled by 'NonLin.') obtained from the partial nonlinear model to the linear numerical ones (labeled by 'Lin.') and the experimental ones (labeled by 'Exp.') with the SES model running speed $U = 5.0\text{m/s}$ in head waves of wavelength $\lambda = 14\text{m}$. Both of numerical results and experimental data were filtered using a zero-phase lowpass Butterworth filter to eliminate the high frequency ($f \geq 4\text{Hz}$) noise.

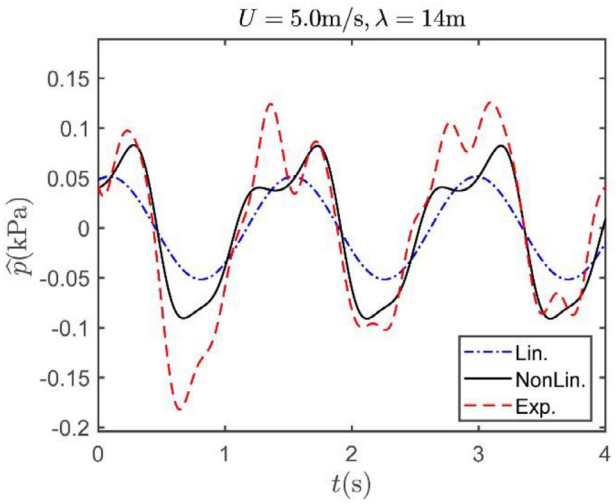

(e) Fluctuating air pressure in the time domain

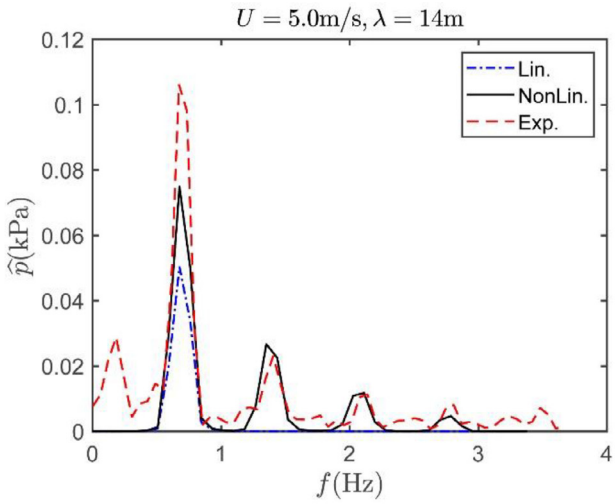

(f) Fluctuating air pressure in the frequency domain

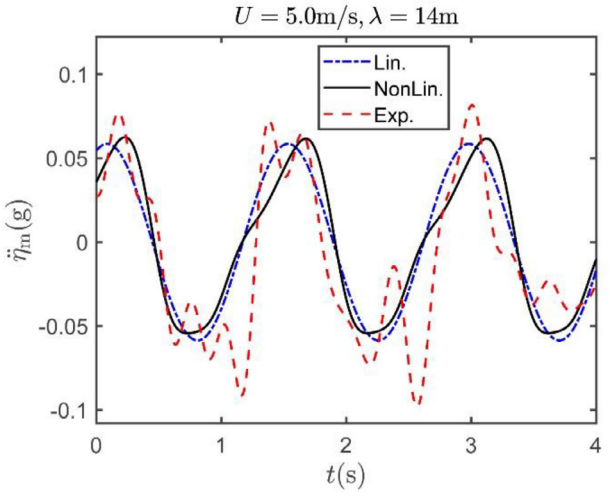

(g) Midship acceleration in the time domain

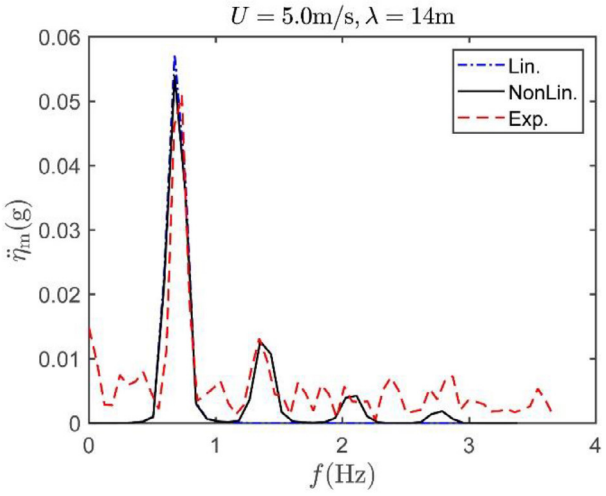

(h) Midship acceleration in the frequency domain

Fig. 8. Continued

drops when the SES moves upward and air leakage gaps open. In contrast, when the SES moves downward and the air leakage gaps are closed, the air pressure rapidly grows and reaches its crests. More details about the influence on air dynamics will be discussed in the next sub-section. Fig. 7(g), (h) show that the nonlinear numerical results satisfactorily reveal the trend the midship acceleration response of the SES as compared with experimental ones. One notes from Fig. 7(h) that the triple and quadruple-frequency responses in numerical results appear clearly, while in experimental ones are not so distinct from the frequencies in their vicinity, which implies there might exist more nonlinear effects on the SES dynamics rather than the shutdown effect of air leakage.

From Fig. 8 one can reach almost the same conclusion as from Fig. 7. However, one may note that the amplitude of the fluctuating air pressure at the encountered frequency from the nonlinear numerical result in Fig. 8(f) is significantly closer to the experimental one than the linear one, which suggests the nonlinear model can even improve the linear response of the SES. Indeed there also exists nonnegligible discrepancy between nonlinear numerical and experimental results. The discrepancy on the fluctuating air pressure is considered to originate from the simplification of numerical models, e.g. the bow and stern skirt dynamics are not taken into account.

Nonetheless, from Fig. 7-8 it can be concluded that the shutdown effect of air leakage is the main resource of nonlinear effects, with which the partial nonlinear model can desirably predict the nonlinear air cushion dynamics as well as the motion response of the SES.

4.2. The factors influencing air dynamics

It can be seen that the air dynamics, which plays important role in the SES dynamics, is vulnerable to factors such as the shutdown on air leakage. In fact, there are two key factors influencing the air dynamics (air pressure). One is the variation of air cushion volume, and the other is the variation of air mass in the cushion. The variation of air cushion volume can be calculated with the consideration of the internal free surface elevation and motions of the SES. The variation of air mass in the cushion can be obtained by counting the difference between air inflow and air leak-

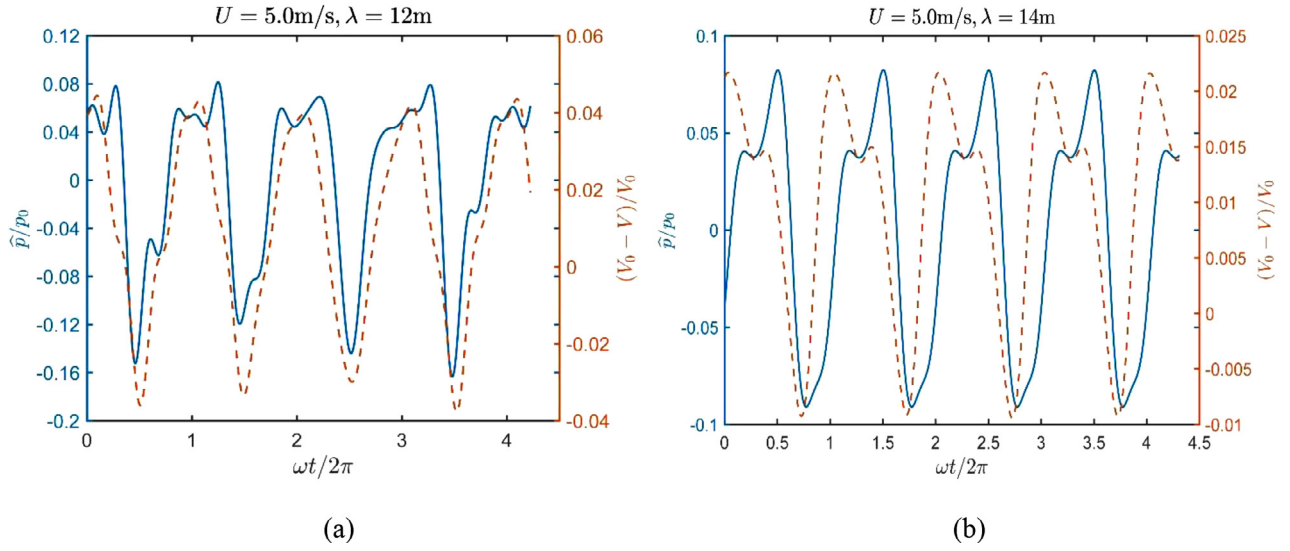

Fig. 9. Comparison of the fluctuating air pressure (blue lines, corresponding to the left *y*-axis) with the variation of air cushion volume (brown dash lines, corresponding to the right *y*-axis) obtained from the partial nonlinear model.

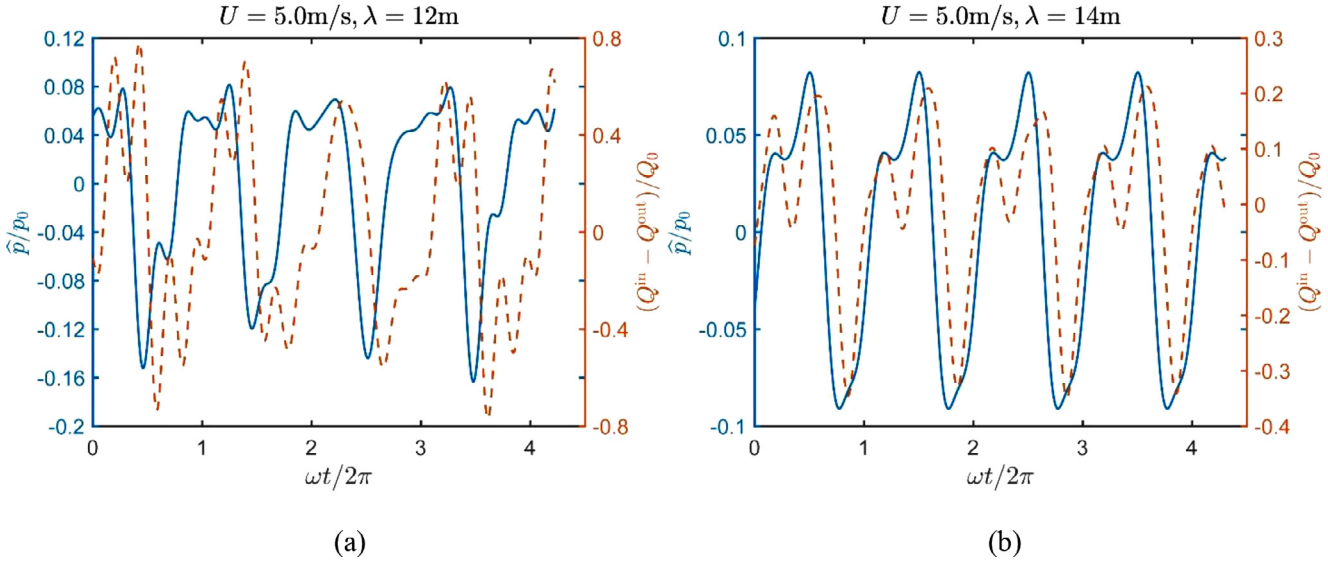

Fig. 10. Comparison of the fluctuating air pressure (blue lines, corresponding to the left *y*-axis) with the air mass increasing rate (brown dash lines, corresponding to the right *y*-axis) obtained from the partial nonlinear model.

age (hereinafter referred to as "air mass increasing rate"). According to Eq. (A17), the air inflow is proportional to the fluctuating air pressure. The air leakage is proportional to the air leakage area (Eq. (4)), which is determined by the motions of the SES. To clearly evaluate the influence on air dynamics, both of the variation of air cushion volume and the variation of air mass are studied in this sub-section.

The variation of air cushion volume can have a significant impact on the air dynamics, and the cobblestone effect is a classical example caused by the resonance of air pressure due to the variation of air cushion volume [13,21]. Fig. 9 compares the nondimensional fluctuating air pressure (blue lines, corresponding to the left *y*-axis) with the variation of air cushion volume (brown dash lines, corresponding to the right *y*-axis) obtained by the partial nonlinear model. The fluctuating air pressure $\hat{p}$ is nondimensionalized by the mean overpressure p_0. The variation of air cushion volume defined as $V_0 - V$ is nondimensionalized by V_0, where V, V_0 are the real time air cushion volume, air cushion volume at equilibrium state, respectively. Fig. 9(a) shows the similar trend between the variation of air cushion volume and the fluctuating air pressure. In Fig. 9(b) the variation of air cushion volume has a phase lead relative to the fluctuating air pressure.

The variation of air mass in the cushion, or the air mass increasing rate, is the other important factor that can influence the air dynamics. The air leakage is the only difference between the partial nonlinear and the linear model in this work, where the former considers the shutdown effect on air leakage (Eq. (5)), i.e., the air leakage area must be nonnegative, while the latter does not have this restriction and negative leakage area may appear. The negative leakage area can lead to an unrealistic phenomenon, i.e., air flows from atmosphere to air cushion, although the pressure of latter is greater than the former.

Fig. 10 presents the influence of air mass increasing rate on the fluctuating air pressure. In Fig. 10, the air mass increasing rate is nondimensionalized as $(Q^{\text{in}} - Q^{\text{out}})/Q_0$, where Q^{in}, Q^{out} *and* Q_0 are the real time air inflow, real time air leakage and the air leakage at equilibrium state, respectively. Fig. 10(a) displays that the air mass increasing rate has a phase lag relative to the fluctuating

air pressure, while in Fig. 10(b) the two variables almost have the same phase.

From Fig. 9 and Fig. 10 it can be concluded that both of the variation of air cushion volume and air mass have positively correlated with the fluctuating air dynamics, and the fluctuating air dynamics might not always be able to simultaneous vary with them.

5. Conclusions

In this paper, an efficient partial nonlinear numerical model was developed for predicting the air dynamics and seakeeping performance of an SES running in small-amplitude waves. The partial nonlinear numerical model comprises a linear frequency domain hydrodynamic model based on the efficient 2.5D method and a nonlinear time domain air dynamic model. The air dynamic model is nonlinear due to the consideration of the shutdown effect on air leakage, i.e., the air leakage area turns zero when the seals are submerged in water. The presented model has advantage of simplicity but holds the key nonlinear feature of the SES.

The experimental results suggest that even in small-amplitude waves, the fluctuating air pressure of the SES shows significant nonlinear effect. The numerical results from the partial nonlinear model, including the linear and nonlinear components of fluctuating air pressure, heave, pitch and midship acceleration, agree well with experimental ones. The investigation demonstrates the effectiveness of the partial nonlinear model on predicting the SES seakeeping motion and on capturing the nonlinear air dynamics. It is also confirmed that nonlinearity of the SES seakeeping performance mainly originates from the nonlinear air leakage. The presented partial nonlinear model can be applied to the more general type of SES with large air cushion displacement proportion (e.g. 80%), while the linear model [10] that cannot capture the nonlinear air dynamics is only applicable to the small proportion one.

Declaration of Competing Interest

The authors declare that they have no known competing financial interests or personal relationships that could have appeared to influence the work reported in this paper.

Acknowledgments

This project is supported by the National Natural Science Foundation of China (Grant no. 52271339, no. 52171289 and no. U22A2012), and Natural Science Foundation of Guangdong Province, China (2021A1515011771).

Appendix A. The air dynamic model

Before modeling the air dynamics, several assumptions or simplifications are made as follows.

(1) The air in the cushion is assumed ideal compressible, and the change of air state is an adiabatic process, which yields the pressure (p) –density (ρ) relationship

$$\frac{p}{\rho^{\gamma}} = \text{Const} \tag{A1}$$

and

$$\rho c^2 = \gamma p \tag{A2}$$

where $\gamma = 1.4$ is the ratio of specific heat capacities for air, c is the local sound speed.

(2) In waves of small-amplitude, the fluctuating air cushion pressure ($p(x, y, z, t)$) is assumed to be much less than the mean overpressure of air cushion (p_0), while the later is much less than the pressure of atmosphere (p_a), i.e.

$$p(x, y, z, t) \ll p_0 \ll p_a \tag{A3}$$

Obviously, when the SES locates at its steady state, the air cushion pressure is $p_a + p_0$.

(3) It is assumed that the length l and width b of the air cushion is much larger than its height h, i.e., $l, b \gg h$, and the variation of the fluctuating air pressure in the cushion along the vertical direction is not significant, then the fluctuating air cushion pressure$p(x, y, z, t)$can be approximated to

$$\hat{p}(x, y, t) \cong \frac{1}{h}\int_0^h p(x, y, z, t)\mathrm{d}z \tag{A4}$$

(4) The sidewall and end seals of the air cushion can be deemed as vertical boundaries, where air cannot penetrate through [19]. Then, according to the momentum equation

$$\hat{\rho}_a \frac{\mathrm{d}\boldsymbol{v}}{\mathrm{d}t} = -\nabla \hat{p} \tag{A5}$$

one obtains

$$\begin{cases} \frac{\partial \hat{p}}{\partial x} = 0, & x{=}x_m \pm \frac{l}{2},\ y_m - \frac{b}{2} < y < y_m{+}\frac{b}{2},\ z_i < z < z_h \quad \text{(a)} \\ \frac{\partial \hat{p}}{\partial y}{=}0, & x_m - \frac{l}{2} < x < x_m{+}\frac{l}{2},\ y = y_m \pm \frac{b}{2},\ z_i < z < z_h \quad \text{(b)} \end{cases} \tag{A6}$$

where $\boldsymbol{v} = (u, v, w)$ is the air velocity, $\hat{\rho}_a$ the air density in the cushion, $(x_m,\ y_m)$ the coordinate of the horizontal center of the air cushion, $z_i,\ z_h$ are the z-th coordinate of the interface (the free surface under air cushion) and the wetted surface, respectively.

(5) It is further assumed that the wavelength is much longer than the air cushion length, and then the air pressure in the cushion can be considered to be uniform, i.e. the acoustic resonance does not occur.

Now, we start to model the air dynamics based on the above-mentioned assumptions.

- *Wave equation for the fluctuating air pressure*

Taking the boundary conditions (Eq. (A6)) into account, the fluctuating air cushion pressure on the interface can be expressed as

$$\hat{p}(x, y, t) = -\rho_w g \sum_{j=8}^{7+N_p} \eta_j(t) n_j(x, y) \tag{A7}$$

where ρ_w is the density of water, $\eta_j(t)$ the waterhead, N_p the number of modes of the fluctuating air pressure, g the gravitational acceleration, $n_j(x, y)$ a complete set of orthogonal Fourier modes expanded on the interface defined as [10,16]

$$n_j(x, y) = \begin{pmatrix} \cos(\alpha\pi(x - x_m)/l) \\ \sin(\alpha\pi(x - x_m)/l) \end{pmatrix} \begin{pmatrix} \cos(\beta\pi(y - y_m)/b) \\ \sin(\beta\pi(y - y_m)/b) \end{pmatrix} \tag{A8}$$

where α, β are 0 and even for the modes corresponding to the cosine or odd for the sine, $x_m,\ y_m$ the longitudinal and transversal center of the air cushion, respectively.

The fluctuating air pressure $p(x, y, z, t)$ in the cushion satisfies the wave equation

$$\frac{\partial^2}{\partial t^2} p(x, y, z, t) - c^2 \nabla^2 p(x, y, z, t) = 0 \tag{A9}$$

Replacing $p(x,y,z,t)$ in Eq. (A4) by Eq. (A9) comes to

$$\left(\frac{\partial^2}{\partial t^2}-c^2\left(\frac{\partial^2}{\partial x^2}+\frac{\partial^2}{\partial y^2}\right)\right)\hat{p}(x,y,t)=\frac{c^2}{h}\left(\frac{\partial p}{\partial z}\Big|z=z_h\right)\Big|z=z_i \tag{A10}$$

Substituting Eq. (A7) into Eq. (A10) with the consideration of momentum equation (Eq. (A5)), Eq. (A9) turns to

$$\sum_{j=8}^{7+N_P}\left(\ddot{\eta}_j(t)n_j(x,y)-c^2\eta_j(t)\left(\frac{\partial^2}{\partial x^2}+\frac{\partial^2}{\partial y^2}\right)n_j(x,y)\right)=\frac{\hat{\rho}_a c^2}{\rho_w g h}\dot{w}\Big|z=z_h\Big|z=z_i \tag{A11}$$

where w, $\dot{w}$ are the vertical velocity, acceleration of the air in the cushion, respectively.

According to the pressure-density relationship (Eq. (A2)) and the small fluctuating air pressure assumption (Eq. (A3)), one obtains

$$\hat{\rho}_a c^2=\gamma\left(\hat{p}(x,y,t)+p_0+p_a\right)\cong\gamma(p_0+p_a) \tag{A12}$$

Substituting Eq. (A12) into Eq. (A11), then multiplying Eq. (A11) by $n_i(x,y)$, $i=8,\ldots,7+N_P$, integrating the equation with respect to x,y on the horizontal section of the air cushion, and finally integrating the resulting equation with respect to t, one gets

$$\begin{aligned}&\sum_{j=8}^{7+N_P}\left(\dot{\eta}_j(t)+\pi^2c^2\left(\left(\frac{\alpha}{l}\right)^2+\left(\frac{\beta}{b}\right)^2\right)\int\eta_j(t)\mathrm{d}t\right)\\&\times\iint_{S_P}n_i(x,y)n_j(x,y)\mathrm{d}x\mathrm{d}y=\frac{\gamma(p_0+p_a)}{\rho_w g h}\\&\times\left(\iint_{S_D}n_i(x,y)w\mathrm{d}x\mathrm{d}y-\iint_{S_P}n_i(x,y)w\mathrm{d}x\mathrm{d}y\right)\end{aligned} \tag{A13}$$

where S_D, S_P are the wetted deck and interface, respectively.

According to the uniform air pressure assumption, only the first Fourier mode is needed in this paper, i.e. $N_P=1$, $\alpha=\beta=0, n_8(x,y)=1$, $\hat{p}(x,y,t)=\hat{p}(t)=-\rho_w g\eta_8(t)$. Thereby, Eq. (A13) comes to

$$\begin{aligned}\dot{\eta}_8(t)A=\frac{\gamma(p_0+p_a)}{\rho_w g h}\Big(A\Big(&\dot{\eta}_3(t)+(y_m-y_g)\dot{\eta}_4(t)\\&-(x_m-x_g)\dot{\eta}_5(t)-\bar{\bar{\zeta}}(t)\Big)-(Q^{in}(t)-Q^{out}(t))\Big)\end{aligned} \tag{A14}$$

where $A=lb$ is the horizontal area of the air cushion; $\eta_i(t)$, $i=1,2,\ldots,6$ are the surge, sway, heave, roll, pitch, yaw of the SES, respectively; Q^{in}, Q^{out} are the air inflow into the cushion and air leakage out of the cushion, respectively; $\bar{\bar{\zeta}}(t)$ is the averaged interface elevation velocity, which is the joint result of incident wave, side hull radiation and diffraction waves and fluctuating air pressure radiation wave, i.e.

$$\bar{\bar{\zeta}}(t)=\frac{1}{A}\iint_{S_P}\frac{\partial}{\partial t}\zeta(x,y,t)\mathrm{d}x\mathrm{d}y \tag{A15}$$

$$\begin{aligned}\zeta(x,y,t)&=-\frac{\hat{p}(x,y,t)}{\rho_w g}-\frac{1}{g}\left(\frac{\partial}{\partial t}-U\frac{\partial}{\partial x}\right)\phi_T\\&=\eta_8(t)-\frac{1}{g}\left(\frac{\partial}{\partial t}-U\frac{\partial}{\partial x}\right)(\phi_I+\phi_R+\phi_D+\phi_P)\end{aligned} \tag{A16}$$

where U is the sailing speed of the SES, $\phi_T=\phi_I+\phi_R+\phi_D+\phi_P$ is the unsteady disturbance potential of water around the SES, ϕ_I, ϕ_R, ϕ_D, ϕ_P are the potential of incident wave, side hull radiation wave, side hull diffraction wave and the radiation wave due to fluctuating air pressure, respectively. The approaches for determining these potentials will be described in the next subsection.

- *Air inflow into the cushion*

The air inflow into the cushion is caused by fans. Although the air pressure was considered to be proportional to the quadratic of air inflow rate [4,12,21], the linear relation between them also approximately holds if the fluctuating air pressure is sufficiently small [6,20]. Therefore, the air inflow into the cushion can be written as

$$Q^{in}(t)=Q_0+\hat{p}(t)\left(\frac{\partial Q_{in}}{\partial p}\right)_0=Q_0-\rho_w g\eta_8(t)\left(\frac{\partial Q_{in}}{\partial p}\right)_0 \tag{A17}$$

where $\left(\frac{\partial Q_{in}}{\partial p}\right)_0$ is the air discharge rate with respect to pressure.

References

[1] S. Bhushan, M. Mousaviraad, F. Stern, Appl. Ocean Res. 67 (2017) 248–262.
[2] S.B. Connell, M.W. Milewski, B. Goldman, C.D. Kring, Single and multi-body surface effect ship simulation for T-Craft design evaluation, in: Proceedings of the 11th International Conference on Fast Sea Transportation. FAST 2011, Honolulu, Hawaii, USA, 2011, pp. 130–137.
[3] W.E. Cummins, Schiffstechnik 9 (1962) 101–109.
[4] L.J. Doctors, The effect of air compressibility on the nonlinear motion of an air-cushion vehicle over waves, in: Proceedings of the 11th ONR Symposium on Naval Hydrodynamics. UCL, London, UK, 1976, pp. 373–388.
[5] O. Faltinsen, R. Zhao, *Philos. Trans. R. Soc. Lond, A* 334 (1991) 241–252.
[6] O.M. Faltinsen, in: Hydrodynamics of High-Speed Marine Vehicles, 1st ed., Publisher: Cambridge University Press, UK, 2005, pp. 141–163.
[7] J. García-Espinosa, D.D. Capua, B. Serván-Camas, et al., Comput. Method Appl. Mech. Eng. 295 (2015) 290–304.
[8] Z.Q. Guo, Q.W. Ma, J.L. Yang, Ocean Eng 110 (2015) 357–376.
[9] Z.Q. Guo, H.D. Qin, Q.W. Ma, Eur. J. Mech. /B Fluids 72 (2018) 353–363.
[10] Z.Q. Guo, Q.W. Ma, H.D. Qin, Appl. Ocean Res. 78 (2018) 25–32.
[11] Z.Q. Guo, Q.W. Ma, H.D. Qin, Water (Basel) 10 (2) (2018) 232.
[12] O.M. Haukeland, V. Hassani, Ø.F. Auestad, Surface effect ship with four air cushions, Part I: dynamic modeling and simulation, in: Proc. of the 12th IFAC Conference on Control Applications in Marine Systems, Robotics, and Vehicles (CAMS 2019), Daejeon, South Korea, 2019, pp. 128–133.
[13] N. Hirata, O.M. Faltinsen, J. Fluids Struct. 14 (2000) 1053–1069.
[14] C.H. Kim, S. Tsakonas, J. Ship Res. 25 (1) (1981) 44–61.
[15] C.H. Lee, J.N. Newman, Mar. Struct. 13 (2000) 315–330.
[16] C.H. Lee, J.N. Newman, Int. J. Offshore Polar Eng. 1 (2015) 347–353.
[17] S. Ma, W.Y. Duan, J.Z. Song, Ocean Eng 32 (8–9) (2005) 937–960.
[18] Alan V. Oppenheim, Ronald W. Schafer, John R. Buck, Discrete-Time Signal Processing, Prentice Hall, Upper Saddle River, NJ, 1999.
[19] A.J. Sørensen, O. Egeland, Auromadca 31 (2) (1995) 183–199.
[20] N. Xie, D. Vassalos, A. Jasionowski, P. Sayer, Ocean Eng 35 (2008) 1512–1520.
[21] L. Yun, A. Bliault, Theory and Design of Aircushion Craft, Bath Press, London, Great Britain, 2000.
[22] J.L. Yang, H.B. Sun, Z.Q. Guo, *J. Huazhong Univ. Sci. Tech.* (Natural Science Edition) 43 (11) (2015) 104–109.